

Research Article

Understanding the Pathway of Gas Hydrate Formation with Porous Materials for Enhanced Gas Separation

Jia Liu^{1,2}, Yajuan Wei^{1,3}, Wei Meng⁴, Pei-Zhou Li¹, Yanli Zhao^{1,*}, and Ruqiang Zou^{4,*}

¹Division of Chemistry and Biological Chemistry, School of Physical and Mathematical Sciences, Nanyang Technological University, 21 Nanyang Link, Singapore 637371

²Department of Chemistry, School of Science, Tianjin University, Tianjin 300072, China

³School of Chemistry, Nankai University, Tianjin 300071, China

⁴Department of Materials Science and Engineering, College of Engineering, Peking University, Beijing 100871, China

* Correspondence should be addressed to Yanli Zhao; zhaoyanli@ntu.edu.sg and Ruqiang Zou; rzou@pku.edu.cn

Received 19 March 2019; Accepted 23 April 2019; Published 28 May 2019

Copyright © 2019 Jia Liu et al. Exclusive Licensee Science and Technology Review Publishing House. Distributed under a Creative Commons Attribution License (CC BY 4.0).

The reason that the stoichiometry of gas to water in artificial gas hydrates formed on porous materials is much higher than that in nature is still ambiguous. Fortunately, based on our experimental thermodynamic and kinetic study on the gas hydrate formation behavior with classic ordered mesoporous carbon CMK-3 and irregular porous activated carbon combined with density functional theory calculations, we discover a microscopic pathway of the gas hydrate formation on porous materials. Two interesting processes including (I) the replacement of water adsorbed on the carbon surface by gas and (II) further replacement of water in the pore by gas accompanied with the gas condensation in the pore and growth of gas hydrate crystals out of the pore were deduced. As a result, a great enhancement of the selectivity and regeneration for gas separation was achieved by controlling the gas hydrate formation behavior accurately.

1. Introduction

Gas hydrates are a type of ice-like clathrate compounds that existed in nature, which have attracted considerable attention because of their unique properties [1–5] and various applications. For example, artificial gas hydrates are considered one of the most promising materials for gas storage [6–8] and separation [9–11]. The formation of gas hydrates in hydrophobic pores has been widely reported as an effective method to enhance gas hydrate formation kinetics and capacity [12–18]. It has been reported that the stoichiometry of gas to water in artificial gas hydrates formed on porous carbon is much higher than that calculated from the crystal structure [9, 19]. An acceptable hypothesis is that the enhanced gas in artificial gas hydrates is attributed to additional gas adsorption in gaps between formed gas hydrates and pore surface or semiclathrate. However, important questions about what kind of gaps and how they can be formed are still not clarified, because there is no valid scientific method to distinguish this type of gaps and semiclathrate in the pore, and quantitative analysis of the gas in gas hydrates or adsorptive phase is hardly

carried out. Some techniques such as molecular simulations [11, 20], *in situ* Raman spectroscopy [21], solid-state nuclear magnetic resonance [10, 22], neutron diffraction [23, 24], and synchrotron X-ray powder diffraction [25] could only be employed to confirm that the formation of gas hydrates is dependent on porous materials. There is no doubt that gas hydrates could be formed on porous materials, but the details about the formation process and whether they are formed inside the pores or not are still ambiguous.

A common understanding is that porous materials could be employed to enhance the gas hydrate formation due to the nanoconfinement effect. After the clusters of gas hydrates form in the nanoconfined space, blank space appears to allow for the gas occurrence as shown in Figure 1. Due to lack of convincing characterization techniques, however, the formation of gas hydrates in the confined space has not been experimentally proven yet. In comparison with this classic mechanism, we discovered a different process (I–IV in Figure 1) for the gas hydrate formation based on the investigation of CO₂ hydrate formation on porous carbon. In this case, when CO₂ was introduced into porous carbon

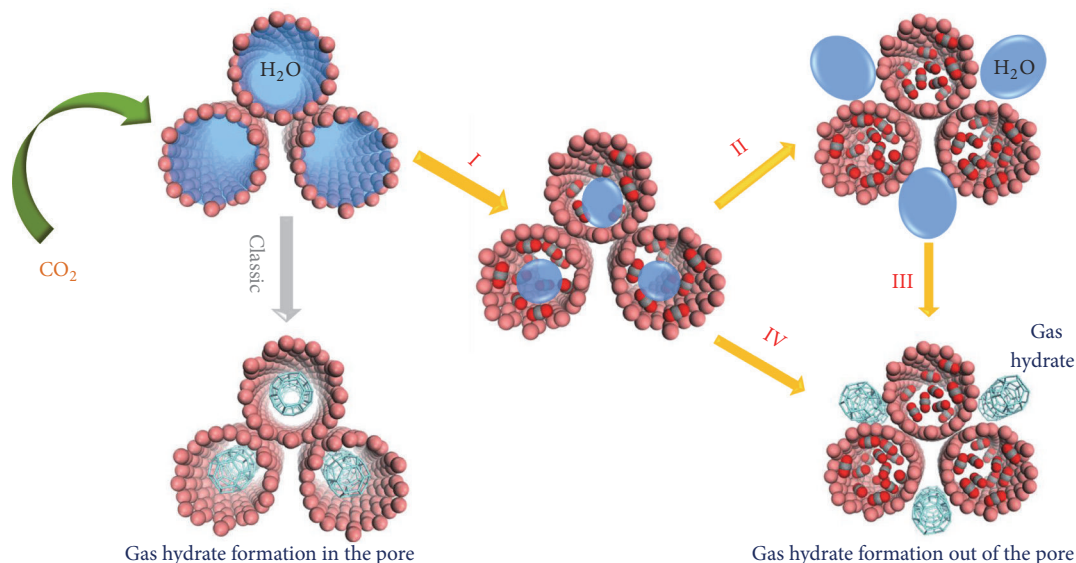


FIGURE 1: Gas hydrate formation based on porous materials. (I-IV) Replacing water by CO_2 on the surface and in the pore, and large gas hydrate crystals are formed outside the pore.

fully filled with water, the considerable sorption of CO_2 was observed on account of a consequence of interesting processes including (I) the replacement of water adsorbed on the carbon surface by CO_2 and (II-IV) further replacement of water in the pore by CO_2 accompanied with the growth of gas hydrate crystals out of the pore.

In process (I), although the calculated binding energy of $\text{C}-\text{CO}_2$ is slightly weaker than that of $\text{C}-\text{H}_2\text{O}$, a portion of water directly adsorbed on the carbon surface could still be replaced by CO_2 driven by the entropy. During the process (II), the water inside the pore is further replaced by CO_2 upon increasing CO_2 chemical potential. Finally, gas hydrates are formed outside the confined space, and CO_2 is condensed in the pore by route III. The gas hydrates could also be formed by following another route (IV). When the pressure reaches the value for the CO_2 hydrate formation, microhydrate crystals initially form in the nanoconfined space and then move out to grow into large crystals in order to decrease the surface free energy. Meanwhile, the CO_2 adsorption and condensation occur in the pore. Therefore, it was deduced that the gas hydrates could not be formed in the nanoconfined space. The excess gas observed in artificial gas hydrates resulted from the gas adsorption and condensation in the nanoconfined space when water is driven to form gas hydrates outside the pore. To confirm this assumption, we designed a rigorous experiment to investigate the gas hydrate formation behavior in the nanoconfined space and achieved a novel understanding about the formation behavior of gas hydrates on porous carbon materials. The pathway is totally different with previous hypothesis of the gas hydrate formation inside nanopores. Furthermore, a great enhancement of the selectivity and regeneration for the gas separation on porous materials was achieved based on the mechanism we proposed.

2. Results

We selected CO_2 as a representative gas for the study. The adsorptive CO_2 could be condensed in confined space with a constant density easy for quantitative analysis. Thus, the CO_2 hydrate formation on classic ordered mesoporous carbon CMK-3 and irregular porous activated carbon (AC) was investigated by thermodynamic experiments, thermodynamic calculations, kinetic analysis, density functional theory (DFT) calculation, and *in situ* Raman spectroscopy. The porous properties calculated from N_2 isotherm curves at 77 K (Figures 2(a) and 2(b)) including Brumauer–Emmett–Teller (BET) surface area, DFT pore size, pore volume, and water vapor uptake (Figures S1 and S2) are summarized in Table S1. The pore volumes of CMK-3 and AC are 1.58 and $1.0 \text{ cm}^3/\text{g}$, respectively. CMK-3 presents an ordered mesoporous structure as shown in Figure 2(c). The scanning electron microscopy (SEM) image of AC indicates a layered structure (Figure 2(d)).

When comparing CO_2 isotherms determined on CMK-3 at 273 K with different mass ratios of water to carbon (R_w), obvious differences were observed as shown in Figure 2(e). The CO_2 isotherm on dry CMK-3 presents a type IV isotherm classified by IUPAC, because of the condensation of CO_2 in the mesopore (3.8 nm). When $R_w = 1$ (i.e., the pore is full of water), the CO_2 uptake is obviously lower than that on the dry sample under the pressure $< 15 \text{ atm}$, since adsorptive sites are occupied by water molecule. As compared with the CO_2 sorption curve in water (Figure S3), the slight CO_2 uptake is mainly attributed to the CO_2 adsorption on the carbon surface. Obviously, the carbon material with different water ratios presents similar CO_2 uptake before 15 atm, and the slight difference should be due to the dissolved CO_2 . It was interestingly found that a small step occurred under 15.1 atm

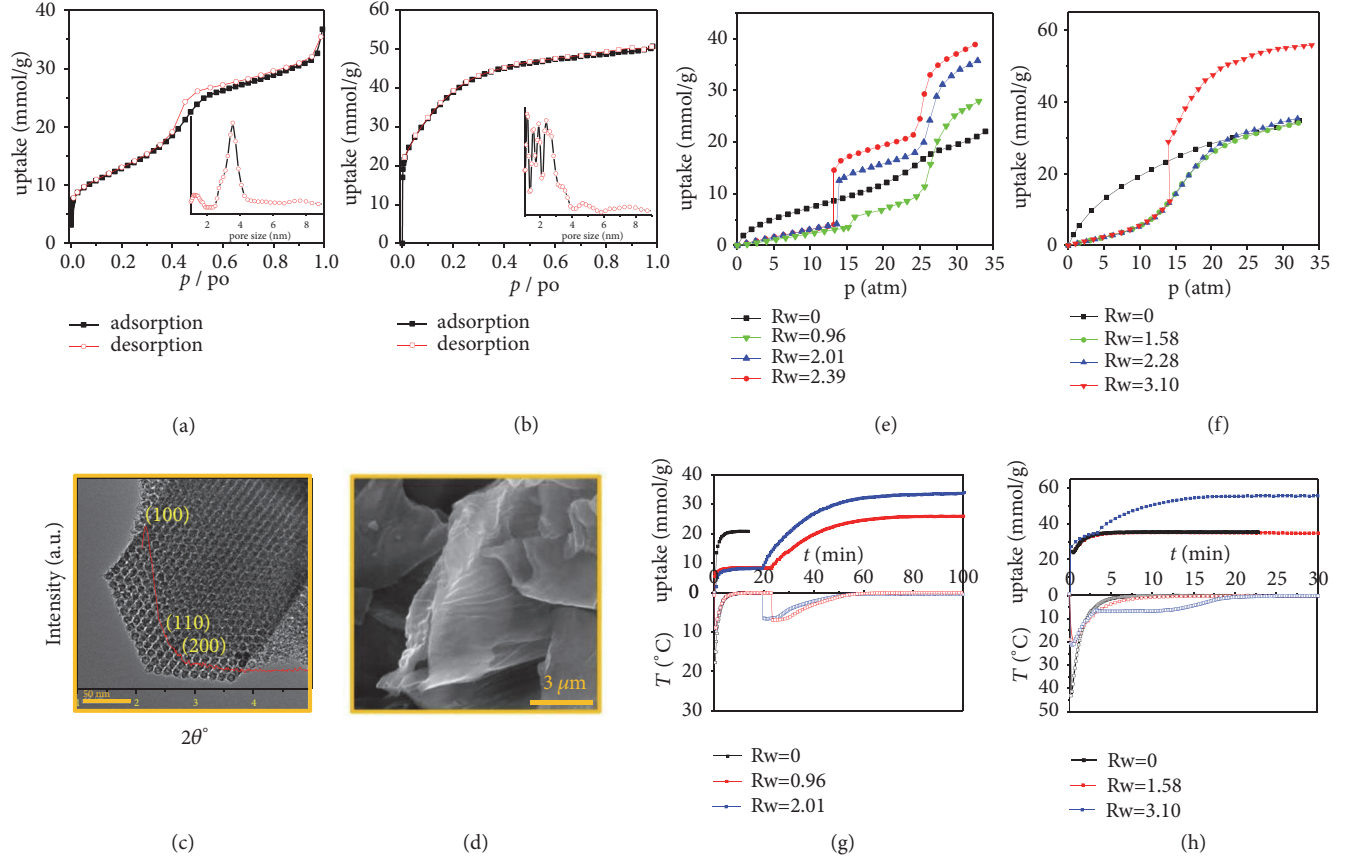


FIGURE 2: Materials characterizations and experimental studies of gas hydrate formation process. N₂ adsorption/desorption isotherms on (a) CMK-3 and (b) AC at 77 K with DFT pore size distribution; (c) TEM image of CMK-3 (inset: powder XRD pattern) and (d) SEM image of AC; CO₂ adsorption isotherms with different water ratios (R_w) at 273 K on (e) CMK-3 and (f) AC; CO₂ dynamic sorption on (g) CMK-3 and (h) AC with different R_w at 273 K with an initial pressure of 30 atm. The filled points are corresponding to CO₂ uptake; blank points are corresponding to temperature.

and a large step happened under pressure > 25 atm. The first step around 14-15 atm observed on all wet CMK-3 should be assigned to the gas hydrate formation. The uptake at the first step increases dependent on the R_w value obviously. When $R_w > 1$, water would overflow the pore volume and occupy the gap of the particles to form the gas hydrates under relatively lower pressure comparing with the formation in the confined space. Based on the equation $dG = -SdT + VdP + \lambda dA$, the smaller the gas hydrate crystal form, the higher the excess surface Gibbs free energy. According to the equation $(\partial G/\partial p)_T = V$, a higher formation pressure is needed when small crystal forms. Similar gas hydrate formation pressure on the porous material to that in bulky water system implies that the gas hydrates are formed out of the pore.

The second step that occurred at relatively higher pressure should be attributed to the gas hydrate formation. However, it was noted that the second step had a similar uptake increase no matter what the R_w value was. The molar ratio of water to CO₂ defined as x was listed in Table 1. It is obvious that the x value (7.67) is higher than the theoretical one (5.75) when water is completely converted into the CO₂ hydrate. The reason is that 5¹² small cages are preferably occupied

by water molecule, and only 6 large cages are retained for CO₂ in a unit cell. In past, this excess uptake was attributed to (1) excess adsorption in the gap between the gas hydrate and carbon surface or (2) the formation of incomplete cages. In the present case, we propose more feasible mechanism that the excess uptake comes from the CO₂ condensation in the mesopore of CMK-3, where water is replaced by CO₂. This mechanism is also supported by other experimental results. When $R_w = 2.01$ (Figure 2(e)), water outside the pore is firstly converted to the CO₂ hydrate under relatively lower pressure of 14 atm at 273 K. With pressurizing CO₂, fragments of water clusters start to form in the pore in order to reduce the surface Gibbs free energy. These fragments and microcrystals tend to combine and grow up out of the pore. However, no sharp increase of uptake could be found under this condition, indicating that the migration of gas hydrate fragments cannot occur independently, unless accompanied with the CO₂ condensation in the mesopore. Cooperating with the CO₂ condensation, the water cluster migrates from inside pore to outside for further growth of the CO₂ hydrate crystals. Meanwhile, the pore gradually becomes empty and allows for the CO₂ condensation to occur. By

TABLE 1: CO₂ uptake during the gas hydrate formation process and corresponding hydrate number.

| Sample | R_w | Uptake | | | | | Molar ratio of water to gas | | |
|--------|-------|--------------|-------------------|-------------------|-------------------|-------------------|-----------------------------|-----------|-----------|
| | | Total uptake | Adsorptive amount | GH _{1st} | GH _{2nd} | GH _{tol} | x_{tol} | x_{1st} | x_{2nd} |
| C1 | 0 | 21.1 | 21.1 | - | - | 0 | - | - | - |
| C2 | 0.96 | 27.9 | 21.1 | 1.38 | 5.45 | 7.83 | 7.80 | 7.85 | 7.65 |
| C3 | 2.01 | 35.6 | 21.1 | 8.72 | 6.05 | 14.77 | 7.64 | 7.23 | 7.79 |
| C4 | 2.39 | 38.8 | 21.1 | 12.50 | 5.23 | 17.43 | 7.48 | 7.96 | 7.29 |
| A1 | 0 | 37.1 | 34.0 | 0 | 0 | 0 | - | - | - |
| A2 | 1.58 | 34.6 | 34.0 | 0 | 0 | 0 | - | - | - |
| A3 | 2.28 | 35.0 | 34.0 | - | - | - | - | - | - |
| A4 | 3.10 | 56.5 | 34.0 | - | - | 22.50 | 7.65 | - | - |

GH_{1st}, GH_{2nd}, and GH_{tol} correspond to the uptake that resulted from the gas hydrate formation in the first step, second step, and sum of the two steps, respectively. x_{1st} , x_{2nd} , and x_{tol} are the gas hydrate numbers corresponding to the formed gas hydrate in the first step, second step, and sum of the two steps, respectively.

comparing the CO₂ uptake under the two steps and the CO₂ adsorption amount on dry carbon (Table 1), it is clear that the mechanism we proposed here is reasonable. When subtracting the adsorptive amount of CO₂ from the total uptake, the gas hydrates obtained on all wet CMK-3 show reasonable x value to the theoretical one. The result could also be obtained from the desorption branch of isotherm curves. As shown in Figure S4, the desorption branch of CO₂ on CMK-3 ($R_w = 0.96$) shows an obvious hysteresis loop, which is much different from the desorption branch of CO₂ on dry CMK-3. To make it clearer, the estimated gas hydrate amount formed on CMK-3 (6.83 mmol/g) was deducted from the desorption branch. It was found that, when the pressure is >23.7 atm, the desorption branch meets well with that on dry CMK-3, indicating a similar desorption mechanism. When the pressure is decreased, the CO₂ uptake on wet CMK-3 decreases more quickly than that on dry sample. During this step, the gas hydrate decomposes into free water molecule to reoccupy the pore of CMK-3 and accelerate the CO₂ desorption. When calculating the CO₂ uptake by desorption on dry carbon between 12.1-23.7 atm, the released gas amount by gas hydrate decomposition is about 6.91, which is consistent with the value estimated from the adsorption branch.

When similar experiments were carried out on AC with irregular slit pore size around 2 nm, clearly different isotherm curves were obtained. The CO₂ isotherm (Figure 2(f)) on dry AC showed type I curve because of its small pore size (2 nm). Different from the isotherm on wet CMK-3, the CO₂ isotherm on wet AC showed only one inflexion. When the water loading amount is equal to the pore volume, the adsorptive amount exhibits a smooth increase around 15 atm at 273 K, which is very different from the sharp increase at 14 atm observed on wet CMK-3. It is notable that the uptake on wet AC with $R_w = 1.58$ is similar to that on its dry sample. It was deduced that the smooth increase is attributed to the replacement of water by CO₂. When $R_w = 1.58$, the uptake reaches the maximum value on dry AC, indicating that no water is converted to gas hydrates. The same result was observed on AC with $R_w = 2.28$. In this case, although the water loading obviously exceeded the pore volume of AC,

no gas hydrate formation was observed around 14 atm, which was different from the results on CMK-3. The water out of the AC pore cannot form gas hydrates even after 48 h. The reason may be attributed to special porous structure of AC. The pore in AC has a V shape. The water replaced by CO₂ could be located on the top of the V pore, where the pressure for the gas hydrate formation is too high to reach when the CO₂ condensation takes place at the bottom of the pore.

A small hysteresis loop was observed in the desorption branch ($R_w = 2.28$) (Figure S5), which is very different from the CO₂ desorption branch on dry AC, indicating a different desorption mechanism. In this case, the adsorbed CO₂ molecule is easier to depart than that on dry carbon. At 1 atm, the CO₂ desorption could achieve more than 99%. When the pressure decreases, the adsorbed CO₂ dissociates from the surface and is replaced by water molecule. Under the replacement effect of water, the CO₂ dispersion occurs more easily than that on dry AC, attributing to both enthalpy and entropy. On one hand, rebinding of water to carbon surface compensates the enthalpy penalty when CO₂ disperses from the surface. On the other hand, the increase of translation entropy caused by CO₂ desorption is higher than the reduction of translation entropy caused by H₂O adsorption, driving the process proceeding forward. When R_w increases to 3.1, partial water out of the V pore could form gas hydrates at relatively lower pressure, driving water in the pore to participate in the CO₂ hydrate formation. The isotherm curve ($R_w = 3.1$) shows that the sharp increase which occurred at about 15 atm corresponds to the CO₂ hydrate formation. By calculating molar ratio of water to gas, the value of $x = 7.65$ is well consistent with the theoretical one (7.67), indicating that water on AC is completely converted to the gas hydrate under this condition. It was also noticed that, after subtracting the uptake caused by the gas hydrate formation, the isotherm curve ($R_w = 3.1$) is similar to others ($R_w = 1.58$ and 2.28), suggesting that the mechanism of CO₂ adsorption on AC with pressure > 15 atm under different R_w is similar. The desorption branch ($R_w = 3.1$) shows a small hysteresis loop (Figure S5). The sharp decrease of CO₂ uptake occurs at about 13.9 atm corresponding to the hydrate crystal dissociation and CO₂ desorption from the nanopore

accompanied with the reoccupation of water molecule in the nanopore. Similar to the case of CMK-3, the CO_2 dispersion process is promoted by the replacement of water molecule after the gas hydrate decomposition.

In order to distinguish the mechanisms corresponding to the gas uptake obtained from thermodynamically static studies in each step, kinetic adsorptive experiments were carried out. Both of the gas adsorption and hydrate formation are exothermic processes. The gas hydrate formation process is much slower than the adsorption process, because the former includes the inducing period for the nucleation and long period for the crystal growth. Therefore, the inducing period and slow growth rate with heat release are unique features in the hydrate formation. Kinetic curves with temperature changes are shown in Figures 2(g) and 2(h). From the kinetic curve, it was found that temperature peaks which occurred on both materials are accompanied with inflection points of uptake. As compared with blank experiment (Figure S6), when loading CO_2 on dry CMK-3, only one temperature peak around 18°C was observed, attributing to the release of adsorptive heat, gas expanding heat, and heat transferred from the environment. In the case of $R_w = 0.96$ and 2.01 , the first peak of temperature decreases to about 9°C because of high capacity of water. On wet CMK-3, the second inflection point occurs after about 20 min, and slow decline should be attributed to the phase transferring heat.

A similar trend of temperature changes was observed on AC as well. When loading CO_2 on dry AC, the temperature peak reaches about 45°C , which is much higher than that on CMK-3 due to higher adsorptive amount and stronger potential intensity of the pore in AC. When loading CO_2 on wet AC, the first temperature peak decreases to 20°C , because of high heat capacity of water. When $R_w = 1.58$, only one temperature peak corresponding to a sharp uptake increase without inducing time was observed. This is strong evidence for the conclusion that CO_2 hydrates cannot be formed in this case. When $R_w = 3.1$, the peak of temperature around 8°C occurs with relatively longer platform, indicating that the process is accompanied with a slow exothermic process assigned to the gas hydrate formation.

In order to obtain the accurate value of the heat, the isotherm curves (Figures S7-S12) at different temperatures were collected for phase changing enthalpy analysis. According to the Clausius-Clapeyron equation, adsorptive enthalpy on CMK-3 with different R_w was obtained (see Supporting Information for more details). The enthalpy of the first step assigned to the hydrate formation out of pore is 64.7 kJ/mol . The enthalpy of the second step is 31.0 kJ/mol , which is lower than the enthalpy (64.7 kJ/mol) of the CO_2 hydrate formation, but higher than CO_2 condensation enthalpy (19.8 kJ/mol) derived from the CO_2 adsorption on dry CMK-3. Since the enthalpy is not related to the pathway, the enthalpy of the entire process could be calculated from the initial state (gases CO_2 + liquid water) and the final state (condensed CO_2 + CO_2 hydrate). The total calculated enthalpy of the second step is 32.0 kJ/mol , which is amazingly consistent with the value calculated according to the Clausius-Clapeyron equation ($31.0\text{--}32.6\text{ kJ/mol}$). These results further support our conclusion that the condensation

and hydrate formation occur simultaneously at the second step. Similarly, by calculating the enthalpy from isotherm curves on wet AC ($R_w = 3.1$) at different temperatures (Figure S12), the enthalpy of the phase transfer corresponding to the sharp increase of uptake is 68.0 kJ/mol . Similar enthalpy on wet AC (20.0 kJ/mol , $R_w = 1.58$) and on dry AC (23.0 kJ/mol) indicates the same adsorptive mechanism.

It is worth noting that the initial of uptake (8.2 mmol/g) on wet CMK-3 agrees with the adsorptive amount (9 mmol/g) estimated from surface area of CMK-3 ($998\text{ m}^2/\text{g}$), but it is obviously lower than that on dry sample (21 mmol/g). When introducing CO_2 in the system, the first process which happened is that CO_2 replaces part of water adsorbed on the material surface. After the first process, CO_2 molecule adsorbs on the surface of the pore, and the center of the pore is still filled by water molecule. Under experimental pressures with inducing time, the water in the pore is supersaturated by hydrate nucleus. Thus, CO_2 molecule prefers to condense in the center of the pore, and the hydrate nucleus tends to grow up to large crystals. Under these conditions, water in the pore continuously transfers out for the conversion, and CO_2 is continuously condensed in free space. The kinetic curves of wet CMK-3 indicate that the surface adsorption by CO_2 occurs first, and then the gas hydrates are formed along with the CO_2 condensation. The final result is that water in the pore is replaced by condensed CO_2 .

With regard to AC, it is different from CMK-3. The initial adsorptive amount on wet AC ($R_w = 1.58$ and 3.1) is similar to that on dry AC, indicating a complete replacement at first. On CMK-3, initially CO_2 could only replace the water adsorbed on the carbon surface, while, on AC, CO_2 could replace almost all water in the pore. This is because the pore size of these two materials is different. The pore size of AC (2 nm) is smaller than that of CMK-3 (3.8 nm), resulting in stronger potential intensity in the pore of AC and leading to the CO_2 condensation in the pore of AC. As aforementioned, no gas hydrate could be formed on wet AC ($R_w = 1.58$). By increasing water loading amount, it was found that gas hydrates are formed and approach the theoretic hydrate volume. It is understandable that, upon increasing R_w , water is replaced and squeezed out of wedge pore by CO_2 molecule. Part of water out of the pore could form CO_2 hydrates under this condition. It is very interesting that, once the gas hydrates start to form out of the pore, water inside the pore is driven out of the pore to participate in the CO_2 hydrate formation. Comparing with the CO_2 adsorption on CMK-3 having a dependent replacing process with the gas hydrate formation, the replacement on AC could occur anytime, i.e., before, during, or after the gas hydrate formation.

After initial replacement process on CMK-3 and AC, whether water in middle layer of pores is replaced by CO_2 with pressurizing CO_2 is determined by the pore size. In small pores, after initial adsorption of CO_2 on the carbon surface, there is no space for water molecule, and water is squeezed out of the pore completely. When the pore size is large enough for water to occupy middle layer of the pore, the binding energy of $\text{H}_2\text{O-H}_2\text{O}$ and $\text{H}_2\text{O-CO}_2$ is 25 kJ/mol and 19.8 kJ/mol , respectively, calculated by DFT. Obviously,

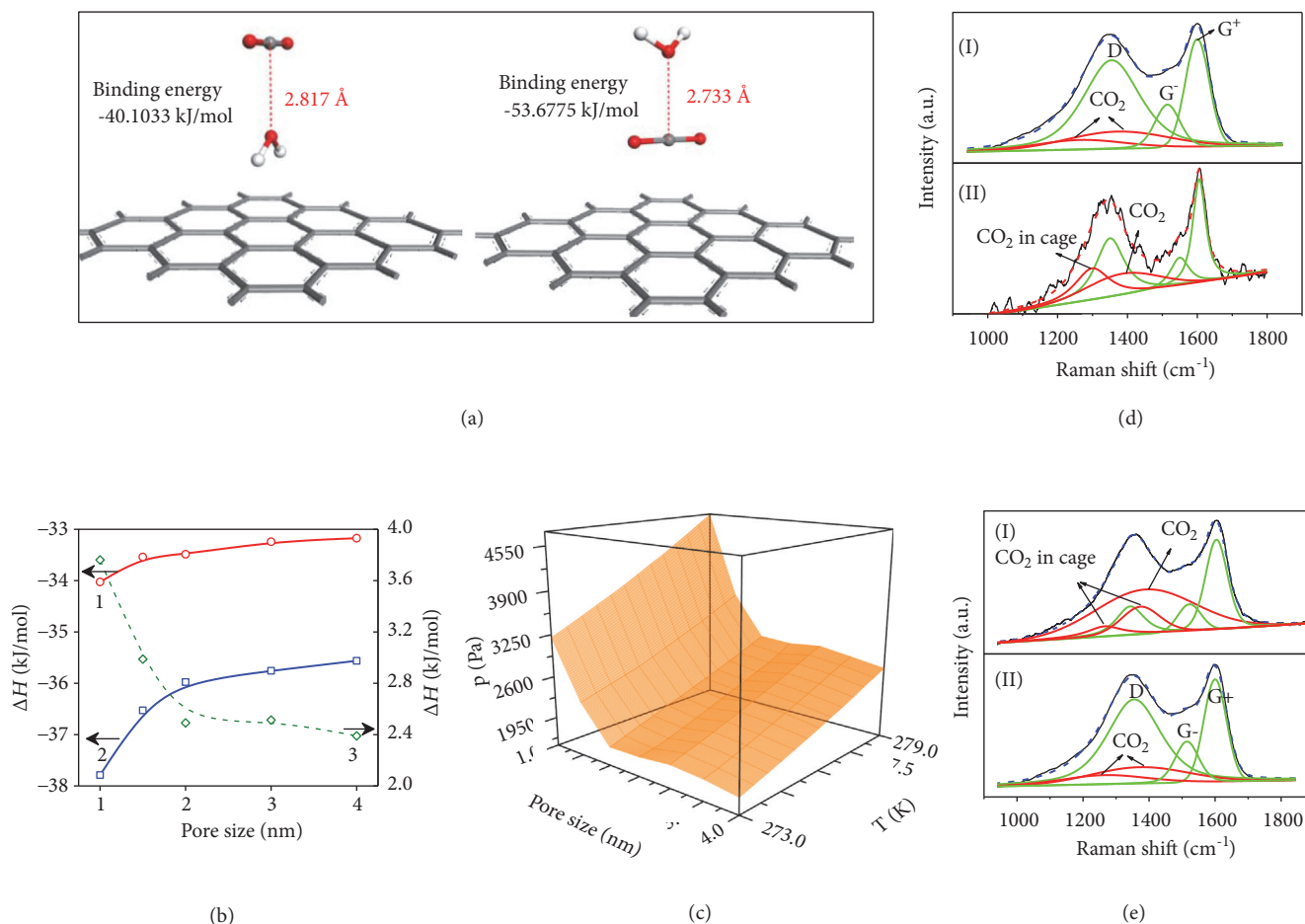


FIGURE 3: Simulation and calculation studies of gas hydrate formation process and in situ Raman studies. (a) Comparison of CO₂-H₂O adsorptive structure on graph (001). (b) Adsorption enthalpy change of water and CO₂ on slit pore model with different pore size: (1) for CO₂; (2) for water; and (3) is the difference of enthalpy between water adsorption and CO₂ adsorption in slit pore with different pore size. (c) Relationship between pressure, pore size, and temperature when the Gibbs energy of the process is less than zero. (d) In situ Raman spectra after (I) loading CO₂ on CMK-3 ($R_w = 1$) immediately and (II) loading CO₂ on CMK-3 ($R_w = 1$) for 8 h. (e) In situ Raman spectra after loading CO₂ on (I) AC-carbon ($R_w = 3.1$) for 8 h and (II) AC-carbon ($R_w = 1.58$) for 8 h.

the CO₂-CO₂ interaction (8.3 kJ/mol) is weaker than that of CO₂-H₂O or H₂O-H₂O, meaning that the CO₂ insertion is not a spontaneous process. To overcome the enthalpy barrier, the CO₂ potential in the gas phase must be enhanced by increasing the CO₂ pressure. When the replacement of water by CO₂ in middle layer of the pore is achieved, CO₂ is located in the pore and condensed. The condensation pressure in 2 nm pore is obviously lower than that in 3 nm pore, since the overlap potential is generated by carbon walls. As observed from static adsorption experiments, the pressure for the water replacement by CO₂ in 2 nm slit pore is about 16 atm. In contrast, in 3.8 nm pore of CMK-3, no replacement could be observed. The pressure inducing this process in 3.8 nm pore is much higher than that for the gas hydrate formation. Therefore, the gas hydrate formation occurs firstly, leading to the transportation of water molecule from inside pore to outside in order to participate in the formation of CO₂ hydrate crystals.

Based on static and kinetic studies, the process of introducing CO₂ in wet carbon systems includes an initial replacement of water by CO₂ on the first layer of carbon surface, the replacement of water in middle layer of the pore, and the formation of CO₂ hydrates. Then, we calculated the entropy, enthalpy, and free energy extracted from ab initio calculations of CO₂-water system confined in layered graphene model with slit size of 1, 1.5, 2, 3, and 4 nm (Figure 3(a)). The replacing process could occur at the carbon surface before the gas hydrate formation, although the carbon atom on the surface of CMK-3 has higher binding energy with H₂O than with CO₂ as shown in Figure 3(b). Therefore, the replacement process of water by CO₂ should be dominated by the entropy.

The entropy of free molecules (CO₂ and H₂O) and adsorbed molecules on the carbon surface and in CO₂ hydrates was calculated from their vibrations (Figures S13 and S14). The total entropy is a sum of translational, rotational, and internal vibrational components: $S_{\text{tot}} = S_{\text{trans}} + S_{\text{rot}} +$

S_{vib} . Six vibration modes of water and CO_2 were obtained, corresponding to bending vibration, symmetric stretching vibration, asymmetric stretching vibration, and rotational vibration. The detailed frequency is listed in Table S2. When comparing the frequency of molecules before and after the adsorption, it was found that obvious changes occur at low frequency region corresponding to rotational vibration. The water rotational vibration is much restricted in carbon pore especially micropore, which accounts for 50% loss of entropy. In contrast, the CO_2 rotational frequency is not changed obviously, meaning that the entropy of water replacement by CO_2 on the carbon surface is favorable, which could compensate the loss of enthalpy. By taking account of the pore size effect, the relationship between pressure, pore size, and temperature when the Gibbs energy of the process is less than zero is shown in Figure 3(c). Obviously, the larger the pore size and the higher the temperature, the higher the pressure needed to make Gibbs free energy less than zero. In addition to the entropy-driven mechanism for the replacement process, in large pore, the replacement of H_2O by CO_2 in single layer region could be spontaneously driven not only by entropy but also by enthalpy. As shown in Figure 3(a), when CO_2 molecule is tiled on the carbon (001) mesh along the C-O-C orientation, the π - π stacking interaction enables one side of the π electrons to focus near the carbon surface, while the opposite side of π electrons is weakened, leading to the situation that lone pair electrons from the $\text{O}_{\text{H}_2\text{O}}$ atom have strong interaction with positively charged C_{CO_2} atom. If lone pair electrons of water directly bind with the surface of carbon, $\text{H}_{\text{H}_2\text{O}}$ must direct to CO_2 molecule. If lone pair electrons of water direct to C_{CO_2} , the π electrons of CO_2 would still have strong interaction with the carbon surface. When compared with the other structure of C- H_2O - CO_2 , simulation results show that the C- CO_2 - H_2O structure is more stable. Thus, the stable configuration makes the replacement of water by CO_2 feasible.

To further confirm the conclusion that CO_2 hydrates could be formed outside the pore under specific conditions, *in situ* Raman studies were performed on CMK-3 and AC. The Raman spectrum of these materials displays characteristic peaks in the spectral range of 1200 to 1800 cm^{-1} . The G feature has a characteristic peak around 1582 cm^{-1} , assigning to all carbon structures having sp^2 hybridization [26]. The band around 1351 cm^{-1} ($\lambda = 532 \text{ nm}$) is known as the D band (defect-induced), and it requires a structural defect to be active in honeycomb carbon lattice. On account of the curvature in contrast to the perfect honeycomb lattice of graphite, the G band splits into the G+ and G- bands centered around 1571 and 1593 cm^{-1} , respectively (Figures 3(d) and 3(e)). Then, the *in situ* Raman spectra were collected on CMK-3 with water ratio of 1 ($R_w = 1$). At the initial loading of CO_2 , the CO_2 adsorption occurs quickly according to the kinetic study results, and the Raman spectrum is separated into several parts (Figure 3(d)(I)). The Raman spectrum of CO_2 in adsorptive phase shows symmetric stretching (1286 cm^{-1}) and bending vibration (1389 cm^{-1}). When CO_2 molecule is enclosed by the hydrate network, the spectrum is broadened and red shifted (Figure 3(d)(II)). When the

hydration is completed, symmetric stretching and bending vibration peaks of CO_2 at 1278 and 1386 cm^{-1} shift to 1277 and 1382 cm^{-1} , respectively, assigning to CO_2 vibration in 5¹² cages. Similar changes were observed on AC as well. Symmetric stretching and bending vibration peaks (Figure 3(e)(I)) shift when water loading ratio is 3.1, indicating the CO_2 hydrate formation. At $R_w = 1.58$, no obvious shifts of CO_2 vibration peaks (Figure 3(e)(II)) were observed, indicating no hydrate formation under this loading ratio, which agrees well with earlier experimental results.

Based on our experimental results on both representatives (CMK-3 and active carbon AC) and DFT studies, the mechanism of gas hydrate formation on porous materials has been well revealed. The water coming from the inner pore could occupy the gap between particles, and the formed gas hydrate crystals fill the empty space. The established conclusion not only provides a new theory to the gas hydrate formation on porous materials, but also offers a reference for further application of gas separation.

The water molecule preadsorbed in the nanopore plays the role of recognizer to different gas (Figure 4(a)). After investigating several gas adsorption/desorption isotherms (CO_2 , CH_4 , and C_2H_6 in Figures S15-S17) on wet carbon materials, it was found that the replacing pressure is related to the gas type. In the case of CH_4 , the water in the pore could only be driven out to form gas hydrate crystals out of pore at high pressure. In comparison to CH_4 and C_2H_6 (Figure 4(b)) on AC ($R_w = 1.58$), C_2H_6 could replace water adsorbed in the pore at a relatively low pressure. By utilizing this difference, the enhancement of $\text{CH}_4/\text{C}_2\text{H}_6$ selectivity from 4 (on dry AC) to 24 (on wet AC) was achieved by calculating from the breakthrough curves (Figure 4(c)). Only C_2H_6 could replace the water adsorbed on AC at current experiment conditions on account of its high binding energy and low entropy penalty. Due to the low binding energy in the pore, CH_4 cannot simply replace water, leading to an ultralow adsorptive amount on wet AC in comparison with that on dry AC (Figure S18). It should be noted that our finding here is much different from the gas separation based on gas hydrates. The enhancement of selectivity could only be achieved in the case that gas hydrates do not form. Once gas hydrates form, water would be driven out of pore to form the gas hydrate cluster, which increases methane competitive occupation in the empty pore of AC and the cage of formed gas hydrates. The increased methane uptake would reduce the $\text{CH}_4/\text{C}_2\text{H}_6$ selectivity. Therefore, the enhanced gas separation in our study follows a different mechanism. More importantly, the regeneration time of C_2H_6 on wet AC reduces to 1/6 on dry AC (Figure 4(d)). Thus, by simply using water in the pore, the drawback of regenerating strong adsorptive gas on porous adsorbents that hinders their industrial applications was overcome.

When the C_2H_6 partial pressure decreases, the water molecule could reoccupy the pore to promote desorption of C_2H_6 molecule. This enhancement could also be understood from the entropy change of the whole process. When water molecule is replaced by gas molecule, the entropy penalty should be compensated by the enthalpy. The CH_4 binding

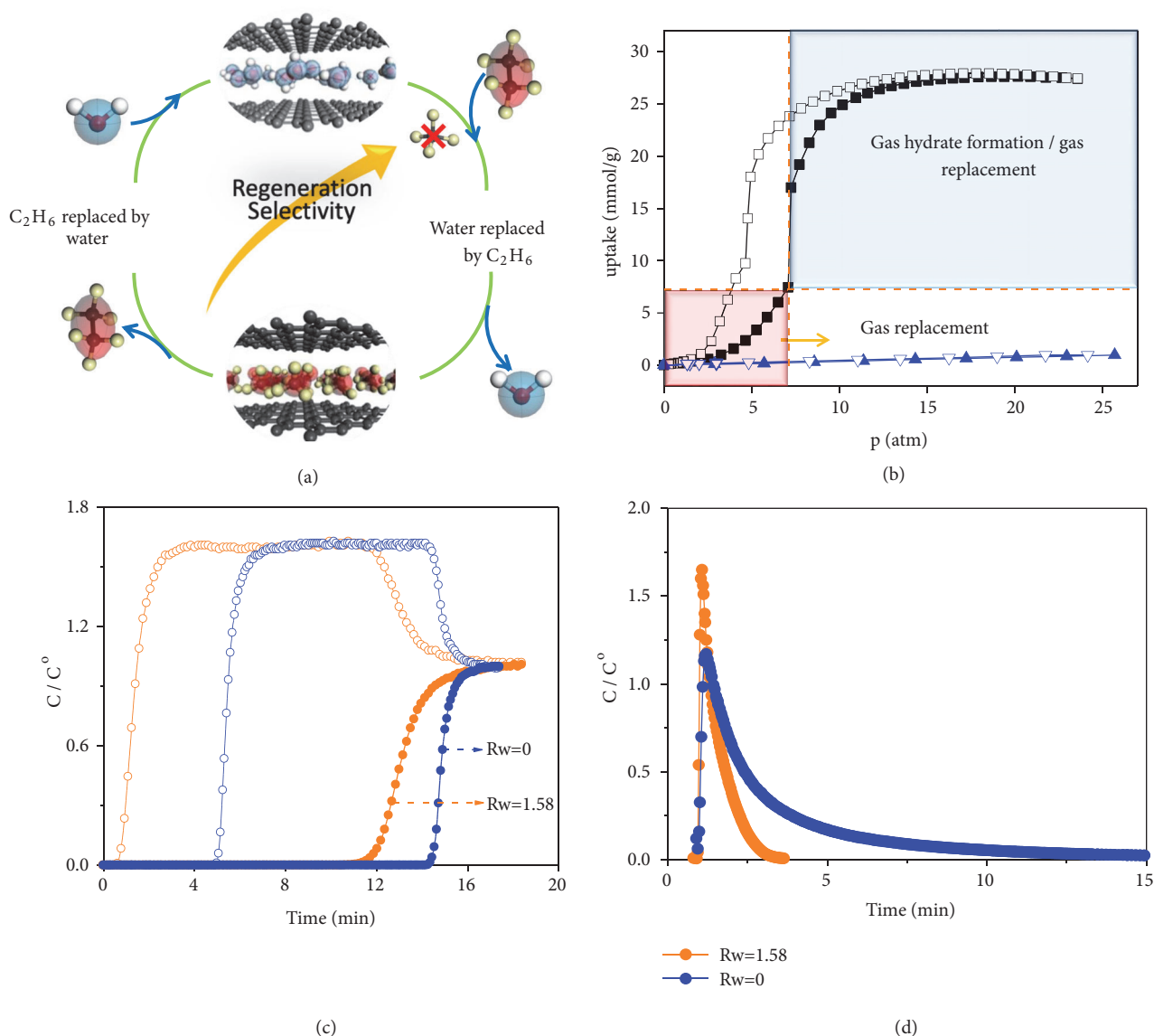


FIGURE 4: Experimental studies of $\text{CH}_4/\text{C}_2\text{H}_6$ separation. (a) Scheme of replacement during the gas adsorption process. (b) Gas isotherm curves on AC at 273 K with $R_w = 1.58$. Blue curve and black curve represent methane and ethane, respectively. The filled symbols represent adsorption branch, and the blank symbols represent desorption branch. (c) Breakthrough curve of $\text{CH}_4/\text{C}_2\text{H}_6$ mixture on AC at 273 K under 1.5 MPa with a flow rate of 100 mL/min. (d) Regeneration curves under atmosphere pressure when purging with N_2 at 273 K with a flow rate of 100 mL/min. In (c) and (d), the filled symbols represent C_2H_6 , and the blank symbols represent CH_4 .

energy (-27.39 kJ) is much lower than that of C_2H_6 (-39.09 kJ) in the pore, so that water could only be replaced by C_2H_6 . During the regeneration process, both of entropy and enthalpy are beneficial to the C_2H_6 desorption and water reoccupation in the pore of AC.

3. Discussion

Based on the thermodynamic and kinetic study on CO_2 adsorption combined with DFT calculations, we have proposed a new mechanism of the gas hydrate formation on

porous materials, which is quite different to previous hypothesis. We have discovered that the gas hydrates could not form and stay in the nanopore, and the excess gas observed in artificial gas hydrates resulted from the gas adsorption and condensation in the nanospace when water is driven out to form gas hydrates out of the pore. The established conclusion not only provides a theory to the gas hydrate formation on porous materials, but also offers a guideline for further application of gas hydrates in the gas separation. The significant improvement of gas selectivity and regeneration could be achieved by controlling the gas hydrate formation process accurately.

According to the new understanding, the method to enhance the gas hydrate formation by using hydrophobic porous materials should be reestimated. Upon the gas hydrate formation on porous materials, the preloaded water could be replaced by adsorbates such as CO_2 , methane, and ethane. Low packing density is always an issue limiting the application of porous materials in the gas storage. Our research by combining the gas storage in the pore and the gas hydrate formation in the empty space overcomes the bottleneck of low packing density and would greatly enhance the gas storage capacity of porous materials under practical conditions. Thus, the present mechanism might be applicable to guide the separation of other binary gas systems.

Data Availability

All data needed to evaluate the conclusions in the paper are present in the paper and the Supplementary Materials. Additional data related to this paper may be requested from the authors.

Conflicts of Interest

The authors declare no conflicts of financial interests.

Authors' Contributions

Jia Liu and Yajuan Wei contributed equally to this work and designed the study, prepared the samples, and performed the thermodynamic and kinetic experiments. Jia Liu carried out DFT calculations. Wei Meng performed Raman experiments. Jia Liu analyzed the data and wrote the paper with contributions from Pei-Zhou Li, Ruqiang Zou, and Yanli Zhao.

Acknowledgments

Ruqiang Zou acknowledges the funding support from the National Natural Science Foundation of China (Grant 51772008). Yanli Zhao is thankful for the support by the Singapore Academic Research Fund (Grants RG5/16, RG11/17, and RG14/17) and the Singapore Agency for Science, Technology and Research (A*STAR) AME IRG grant (Grant A1783c0007).

Supplementary Materials

Method, enthalpy calculation, and thermodynamic calculation and DFT study. Figure S1: N_2 adsorption/desorption isotherms on (a) CMK-3 and (b) AC at 77 K. Insets are DFT pore size distributions. Figure S2: water vapor adsorption/desorption isotherms on dry samples of (a) CMK-3 and (b) AC at 293 K. Figure S3: CO_2 adsorption/desorption isotherms in bulk water at 273 K. Figure S4: comparison of CO_2 adsorption/desorption isotherms on CMK-3 at 273 K. The red blank squares represent the desorption branch after deducting an estimated gas hydrate formation value (6.83 mmol/g) from the real desorption branch. Figure S5: comparison of CO_2 adsorption/desorption isotherms on AC

with different R_w at 273 K. Figure S6: blank experiment of CO_2 adsorptive kinetic temperature curve. Figure S7: CO_2 adsorptive isotherms on CMK-3 at different temperatures when $R_w = 0$. Figure S8: CO_2 adsorptive isotherms on CMK-3 at different temperatures when $R_w = 0.96$. Figure S9: CO_2 adsorptive isotherms on CMK-3 at different temperatures when $R_w = 2$. Figure S10: CO_2 adsorptive isotherms on AC at different temperatures when $R_w = 0$. Figure S11: CO_2 adsorptive isotherms on AC at different temperatures when $R_w = 1.58$. Figure S12: CO_2 adsorptive isotherms on AC at different temperatures when $R_w = 3.1$. Figure S13: vibration modes of adsorbed water molecule and CO_2 on graphene. Figure S14: optimized structures of CO_2 hydrate crystals based on calculations. Red represents oxygen atoms in CO_2 , grey represents carbon atom, and blue and light green represent oxygen and hydrogen in water, respectively. Figure S15: C_2H_6 adsorption/desorption isotherms on AC at 273 K with different R_w values. The filled symbols represent adsorptive branch, and the blank symbols represent desorption branch. Figure S16: C_2H_6 adsorption/desorption isotherms on AC at different temperatures when $R_w = 1.5$. Figure S17: CH_4 adsorption/desorption isotherms on AC at 273 K with different R_w values. The filled symbols represent adsorptive branch, and the blank symbols represent desorption branch. Figure S18: CH_4 and C_2H_6 adsorption/desorption isotherms on dry AC at 273 K. Table S1: physical parameters of samples. Table S2: vibration frequency of free molecules and adsorbed molecules. See References [27–33]. (*Supplementary Materials*)

References

- [1] E. D. Sloan Jr., *Clathrate Hydrates of Natural Gases*, CRC Press, 2nd edition, 1998.
- [2] A. Falenty, T. C. Hansen, and W. F. Kuhs, "Formation and properties of ice XVI obtained by emptying a type sII clathrate hydrate," *Nature*, vol. 516, no. 7530, pp. 231–233, 2014.
- [3] S. Takeya, T. Uchida, Y. Kamata et al., "Lattice expansion of clathrate hydrates of methane mixtures and natural gas," *Angewandte Chemie International Edition*, vol. 44, no. 42, pp. 6928–6931, 2005.
- [4] C. G. Pruteanu, G. J. Ackland, W. C. K. Poon, and J. S. Loveday, "When immiscible becomes miscible-Methane in water at high pressures," *Science Advances*, vol. 3, no. 8, article e1700240, 2017.
- [5] J. Wu, F. Ning, T. T. Trinh et al., "Mechanical instability of monocrystalline and polycrystalline methane hydrates," *Nature Communications*, vol. 6, no. 1, p. 8743, 2015.
- [6] H. Lee, J.-W. Lee, D. Y. Kim et al., "Tuning clathrate hydrates for hydrogen storage," *Nature*, vol. 434, no. 7034, pp. 743–746, 2005.
- [7] M. E. Casco, J. Silvestre-Albero, A. J. Ramírez-Cuesta et al., "Methane hydrate formation in confined nanospace can surpass nature," *Nature Communications*, vol. 6, no. 1, p. 8743, 2015.
- [8] M. E. Casco, F. Rey, J. L. Jordá et al., "Paving the way for methane hydrate formation on metal-organic frameworks (MOFs)," *Chemical Science*, vol. 7, no. 6, pp. 3658–3666, 2016.
- [9] A. S. Jalilov, Y. Li, C. Kittrell, and J. M. Tour, "Increased CO_2 selectivity of asphalt-derived porous carbon through introduction of water into pore space," *Nature Energy*, vol. 2, no. 12, pp. 932–938, 2017.

- [10] H. Lee, Y. Seo, Y.-T. Seo, I. L. Moudrakovski, and J. A. Ripmeester, "Recovering methane from solid methane hydrate with carbon dioxide," *Angewandte Chemie International Edition*, vol. 42, no. 41, pp. 5048–5051, 2003.
- [11] D. Bai, X. Zhang, G. Chen, and W. Wang, "Replacement mechanism of methane hydrate with carbon dioxide from microsecond molecular dynamics simulations," *Energy & Environmental Science*, vol. 5, no. 5, pp. 7033–7041, 2012.
- [12] S. Park, S. Lee, Y. Lee, and Y. Seo, "CO₂ capture from simulated fuel gas mixtures using semiclathrate hydrates formed by quaternary ammonium salts," *Environmental Science & Technology*, vol. 47, no. 13, pp. 7571–7577, 2013.
- [13] A. Siangsai, P. Rangsunvigit, B. Kitiyanan, S. Kulprathipanja, and P. Linga, "Investigation on the roles of activated carbon particle sizes on methane hydrate formation and dissociation," *Chemical Engineering Science*, vol. 126, pp. 383–389, 2015.
- [14] S.-P. Kang and J.-W. Lee, "Formation characteristics of synthesized natural gas hydrates in meso- and macroporous silica gels," *The Journal of Physical Chemistry B*, vol. 114, no. 20, pp. 6973–6978, 2010.
- [15] D. H. Smith, J. W. Wilder, and K. Seshadri, "Thermodynamics of carbon dioxide hydrate formation in media with broad pore-size distributions," *Environmental Science & Technology*, vol. 36, no. 23, pp. 5192–5198, 2002.
- [16] Y. Seo, H. Lee, and T. Uchida, "Methane and carbon dioxide hydrate phase behavior in small porous silica gels: three-phase equilibrium determination and thermodynamic modeling," *Langmuir*, vol. 18, no. 24, pp. 9164–9170, 2002.
- [17] L. Mu, B. Liu, H. Liu, Y. Yang, C. Sun, and G. Chen, "A novel method to improve the gas storage capacity of ZIF-8," *Journal of Materials Chemistry*, vol. 22, no. 24, pp. 12246–12252, 2012.
- [18] J. Liu, Y. Zhou, Y. Sun, W. Su, and L. Zhou, "Methane storage in wet carbon of tailored pore sizes," *Carbon*, vol. 49, no. 12, pp. 3731–3736, 2011.
- [19] Y. Zhou, M. Dai, L. Zhou, Y. Sun, and W. Su, "Storage of methane on wet activated carbon: Influence of pore size distribution," *Carbon*, vol. 42, no. 8–9, pp. 1855–1858, 2004.
- [20] P. Pirzadeh and P. G. Kusalik, "Molecular insights into clathrate hydrate nucleation at an ice-solution interface," *Journal of the American Chemical Society*, vol. 135, no. 19, pp. 7278–7287, 2013.
- [21] J. Wang, H. Lu, and J. A. Ripmeester, "Raman spectroscopy and cage occupancy of hydrogen clathrate hydrate from first-principle calculations," *Journal of the American Chemical Society*, vol. 131, no. 40, pp. 14132–14133, 2009.
- [22] D.-Y. Kim and H. Lee, "Spectroscopic identification of the mixed hydrogen and carbon dioxide clathrate hydrate," *Journal of the American Chemical Society*, vol. 127, no. 28, pp. 9996–9997, 2005.
- [23] S. J. Cox, D. J. F. Taylor, T. G. A. Youngs et al., "Formation of methane hydrate in the presence of natural and synthetic nanoparticles," *Journal of the American Chemical Society*, vol. 140, no. 9, pp. 3277–3284, 2018.
- [24] Y. Halpern, V. Thieu, R. W. Henning, X. Wang, and A. J. Schultz, "Time-resolved in situ neutron diffraction studies of gas hydrate: Transformation of structure II (sII) to structure I (sI)," *Journal of the American Chemical Society*, vol. 123, no. 9, pp. 12826–12831, 2001.
- [25] F. Lehmkuhler, M. Paulus, C. Sternemann et al., "The carbon dioxide-water interface at conditions of gas hydrate formation," *Journal of the American Chemical Society*, vol. 131, no. 2, pp. 585–589, 2009.
- [26] R. D. Rodriguez, M. Toader, S. Hermann et al., "Nanoscale optical and electrical characterization of horizontally aligned single-walled carbon nanotubes," *Nanoscale Research Letters*, vol. 7, no. 1, p. 682, 2012.
- [27] X. Liu, L. Zhou, J. Li, Y. Sun, W. Su, and Y. Zhou, "Methane sorption on ordered mesoporous carbon in the presence of water," *Carbon*, vol. 44, no. 8, pp. 1386–1392, 2006.
- [28] R. Ryoo, S. H. Joo, and S. Jun, "Synthesis of highly ordered carbon molecular sieves via template-mediated structural transformation," *The Journal of Physical Chemistry B*, vol. 103, no. 37, pp. 7743–7746, 1999.
- [29] G. Kresse and D. Joubert, "From ultrasoft pseudopotentials to the projector augmented-wave method," *Physical Review B: Condensed Matter and Materials Physics*, vol. 59, no. 3, pp. 1758–1775, 1999.
- [30] P. E. Blöchl, "Projector augmented-wave method," *Physical Review B: Condensed Matter and Materials Physics*, vol. 50, no. 24, pp. 17953–17979, 1994.
- [31] S. Grimme, J. Antony, S. Ehrlich, and H. Krieg, "A consistent and accurate ab initio parametrization of density functional dispersion correction (DFT-D) for the 94 elements H–Pu," *The Journal of Chemical Physics*, vol. 132, no. 15, article 154104, 2010.
- [32] C. Lechner, B. Pannier, P. Baranek, N. C. Forero-Martinez, and H. Vach, "First-principles study of the structural, electronic, dynamic, and mechanical properties of HOPG and diamond: influence of exchange-correlation functionals and dispersion interactions," *The Journal of Physical Chemistry C*, vol. 120, no. 9, pp. 5083–5100, 2016.
- [33] N. V. Ilawe, J. A. Zimmerman, and B. M. Wong, "Breaking badly: DFT-D2 gives sizeable errors for tensile strengths in palladium-hydride solids," *Journal of Chemical Theory and Computation*, vol. 11, no. 11, pp. 5426–5435, 2015.